electronics

MDPI

Article

A Double-Stage Optimization Approach for Wind Farm Layout Optimization

Faisal Saud Al-Otaibi *, Makbul A. M. Ramli, Yusuf A. Al-Turki and Md. Asaduz-Zaman

Department of Electrical and Computer Engineering, King Abdulaziz University, Jeddah 21589, Saudi Arabia; mramli@kau.edu.sa (M.A.M.R.); yaturki@kau.edu.sa (Y.A.A.-T.); masaduzzaman@stu.kau.edu.sa (M.A.-Z.)
* Correspondence: falotaibi0349@stu.kau.edu.sa

Abstract

Wind farm layout optimization (WFLO) plays a key role in reducing wake effect energy losses and increasing annual energy production (AEP). This paper proposes a double-stage optimization approach that incorporates staggered grid-based optimization with coordinate-based local optimization. In the first stage, staggered grid-based optimization is performed to determine optimal turbine locations within predefined grid boundaries. In the second stage, turbine positions are locally optimized within bounded regions to improve AEP efficiently without extending the search across the entire wind farm. The modified electric charged particle optimization (MECPO) algorithm is applied to evaluate five optimization approaches, including two double-stage and three single-stage approaches. The framework is tested on a wind farm covering an area of 2000 m by 2000 m with 20 turbines under single-direction, uniform multi-directional, and spatially varying wind conditions. The proposed double-stage optimization approach achieves comparable or improved net AEP while significantly reducing computational cost across different wind conditions. The method provides up to 0.36% improvement in net AEP, reduces wake losses by up to 6.84%, and decreases computational time by up to 90% compared with the coordinate-based approach. These results confirm that the proposed approach significantly enhances computational efficiency while maintaining comparable energy performance. The findings indicate that integrating staggered grid-based optimization with coordinate-based local optimization provides an effective balance between solution quality and computational efficiency, offering a practical and scalable approach for WFLO.

Keywords: wind farm layout optimization; double-stage optimization; MECPO algorithm; wake effect; annual energy production; grid-based approach; coordinate-based approach

Check for updates

Academic Editor: Cristina Ventura

Received: 4 May 2026
Revised: 15 May 2026
Accepted: 20 May 2026
Published: 8 June 2026

Copyright: © 2026 by the authors. Licensee MDPI, Basel, Switzerland. This article is an open access article distributed under the terms and conditions of the Creative Commons Attribution (CC BY) license.

1. Introduction

Climate change mitigation has increased global interest in the transition to renewable energy sources [1]. Among these sources, wind energy has become an important option for reducing carbon emissions and decreasing reliance on fossil fuels for electricity generation. In recent years, wind energy has experienced remarkable global growth, reaching 1 TW of installed capacity in 2023, with 117 GW added in that year alone [2]. This expansion is expected to continue, and wind energy is projected to play an increasingly significant role in future global energy supply [3]. As wind energy deployment continues to expand, improving wind farm performance becomes increasingly important. One of the key factors affecting wind farm performance is the arrangement of wind turbines within the available site, which is commonly addressed through wind farm layout optimization (WFLO). The

main objective of WFLO is to determine turbine locations that maximize energy production while satisfying technical and spatial constraints [4]. In addition to reducing energy losses, proper layout design is also important because wake effects can negatively affect both energy production and turbine lifetime through increased loading and wear [5]. WFLO may also be considered from broader economic and environmental perspectives, including cost reduction and environmental impact mitigation such as noise [4,6]. In the literature, WFLO is commonly addressed using two main approaches: grid-based and coordinate-based formulations [7,8]. In the grid-based approach, the wind farm area is divided into cells, and turbines are placed at predefined locations, usually at the cell centers, which simplifies the search process [7]. However, this representation limits placement flexibility [8]. In addition, increasing grid density may improve the chance of identifying better turbine locations, but it also increases computational cost [9]. The literature has highlighted computational cost and scalability as key challenges in WFLO, particularly as the number of turbines increases [10].

Early studies widely adopted grid-based representations to reduce problem complexity. For example, previous works investigated regular grid-based turbine placement using optimization methods such as genetic algorithms and examined its effect on energy production and cost [11,12]. Other studies have also shown that alternative geometric patterns, such as hexagonal and circular arrangements, can improve energy production compared with conventional patterns [13]. By contrast, the coordinate-based approach allows turbines to be placed anywhere within the wind farm boundaries using continuous coordinates, which provides greater flexibility in determining turbine positions [7,14]. This flexibility can improve optimization performance; however, it also enlarges the search space and may increase the computational burden [8,9]. Recent studies have addressed WFLO under complex constraints, with the problem often characterized as a nonlinear and non-convex optimization problem that is computationally demanding [15]. For this reason, coordinate-based and other metaheuristic optimization methods have been extensively used to improve WFLO performance under nonlinear constraints and wake effects [16–18]. Furthermore, recent studies have emphasized the integration of advanced and hybrid optimization techniques to further enhance WFLO performance [19]. More recently, Huang et al. [20] proposed a two-stage grid–coordinate framework in which grid-based optimization is followed by coordinate-based refinement, demonstrating the potential of combining structured configuration with flexible optimization.

Despite these developments, a clear gap remains in the existing literature. Current WFLO studies still exhibit a trade-off between the simplicity of grid-based formulations and the flexibility of coordinate-based formulations [8,9]. Although hybrid or two-stage optimization frameworks have been proposed to combine these approaches [20], they generally rely on conventional square grid without systematically investigating alternative spatial configurations. In particular, the impact of the initial turbine spatial arrangement on the effectiveness of the subsequent optimization stage has not been thoroughly examined. This limitation is critical, as the initial layout plays a key role in guiding the search process and influencing both convergence behavior and final solution quality. Therefore, this study explicitly addresses this gap by investigating the effect of different initial spatial configurations through a systematic comparison between staggered and conventional square grid layouts within a double-stage optimization framework.

Based on the above rationale, the main contributions of this paper are summarized as follows:

- ❖ A double-stage WFLO framework is proposed, combining staggered grid-based and coordinate-based optimization approaches to balance computational efficiency and solution quality.
- ❖ A staggered spatial configuration is introduced as an alternative to the conventional square grid for initial turbine placement.
- ❖ A systematic comparative analysis is conducted under single-direction, uniform multi-directional, and spatially varying wind conditions to evaluate the impact of spatial configuration on optimization performance.
- ❖ The proposed framework is benchmarked against both single-stage and double-stage optimization approaches in terms of AEP, wake effect, and computational time.

The remainder of this paper is organized as follows: Section 2 presents the proposed methodology. Section 3 describes the mathematical modeling. Section 4 introduces the optimization algorithm. Section 5 presents and discusses the simulation results. Finally, Section 6 concludes the paper.

2. Research Methodology

To improve the clarity of the proposed methodology and enhance reproducibility, the overall research methodology for wind farm layout optimization is shown in Figure 1. The framework relies on input data and physical and mathematical models to evaluate wind farm layout performance in a consistent and structured manner. These elements are integrated within a two-stage optimization process implemented using the MECPO algorithm. The process begins by defining the input data, including wind characteristics, wind farm parameters including layout boundaries and available area, turbine specifications, wake model settings, and design constraints. These inputs are used to calculate AEP and assess the performance of different layout configurations. The objective function is defined as the maximization of AEP, which guides the optimization process throughout both stages. The optimization is carried out within a single continuous MECPO run, ensuring a unified search process without interruption. In the first stage, grid-based optimization is performed using a staggered grid. This stage represents a key contribution of the study, as the staggered configuration enhances spatial uniformity and improves the management of wake interactions. A conventional square grid is also considered as a baseline for comparison.

In the second stage, the turbine positions obtained from the first stage are directly used as the initial solutions, ensuring continuity in the optimization process. A coordinate-based refinement is then performed on the turbine positions within the grid boundaries defined by the initial layout, without expanding the search over the entire wind farm area. This constraint is intentionally imposed to reduce the search space and consequently decrease computational time, as full-space exploration significantly increases computational complexity and processing cost. Finally, the framework outputs the optimal wind farm layout along with key performance indicators, including maximum AEP, wake loss, and computational time. In addition, a systematic comparison with single-stage approaches and square grid configuration is conducted to evaluate the effectiveness, robustness, and practical applicability of the proposed framework.

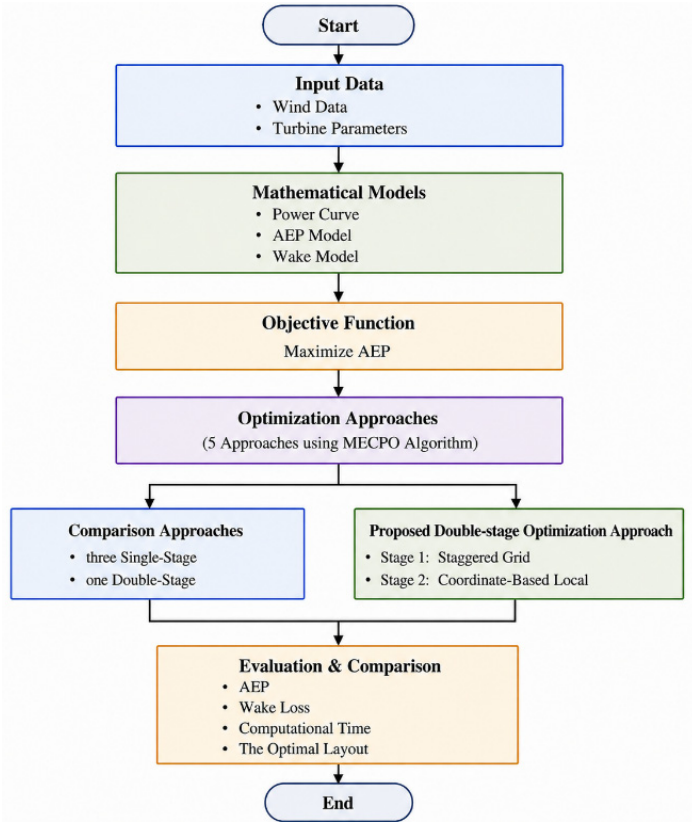


Figure 1. Overall workflow of the research methodology.

3. Mathematical Models for Wind Farm Layout Optimization

This section introduces the mathematical models used to evaluate wind farm performance and guide the optimization process. These models play a crucial role in accurately estimating energy production and capturing the interactions between turbines. The modeling framework includes the wind turbine power curve, the probabilistic calculation of AEP based on wind distributions, and the wake effect model, which represents the reduction in wind speed caused by upstream turbines.

3.1. Wind Turbine Model

The rated power output of a wind turbine is a key factor that directly affects its total energy generation capacity. This value varies from one turbine model to another, along with other specifications such as cut-in speed, rated speed, cut-out speed, rotor diameter, and hub height. An essential tool for accurately estimating energy production is the power curve, which illustrates the turbine's response to varying wind speeds and serves as the basis for determining the AEP. The power output of a wind turbine at each wind speed interval is expressed in Equation (1), while Figure 2 presents the wind turbine power curve.

$$P(v) = \begin{cases} 0 & if\ v < v_{cut\text{-}in} \\ \lambda v + \eta & if\ v_{cut\text{-}in} < v < v_{rate} \\ P_{rate} & if\ v_{rate} < v < v_{cut\text{-}out} \end{cases} \quad (1)$$

When the wind speed exceeds the cut-in speed ($v_{cut\text{-}in}$), a wind turbine (WT) starts to rotate. As wind speed increases, the turbine's power output increases steadily between $v_{cut\text{-}in}$ and the rated speed (v_{rate}). When the turbine reaches v_{rate}, it produces a steady output equal to the rated power (P_{rate}) and keeps it there until the wind speed hits the cut-out threshold ($v_{cut\text{-}out}$); $\lambda v, \eta$ refer to the slope and intercept parameters, respectively [18,21].

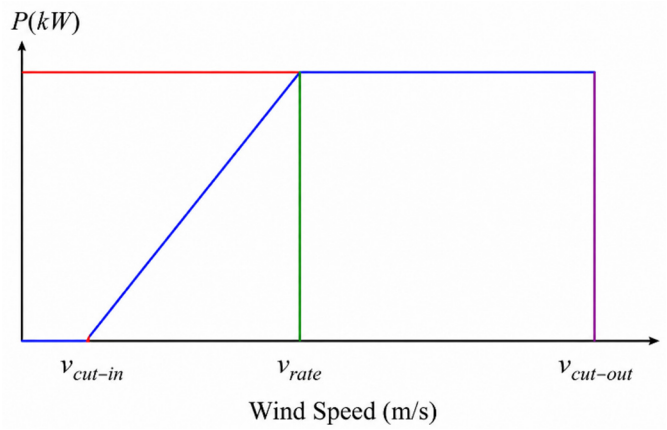


Figure 2. Wind turbine power curve.

3.2. Annual Energy Production Calculation

To calculate the energy production of a wind turbine, a probabilistic formula based on wind speed and direction is adopted, as expressed in Equation (2). The expected energy capture is calculated by integrating the turbine power curve with the wind speed probability density function for each wind direction, as is common in wind farm design optimization studies [18].

$$E = \int_A p(\theta) \int_v p_v(v; c_i; k_i|\theta)\eta(v) \tag{2}$$

In this context $p(\theta)$ and $p_v(v; c_i; k_i|\theta)\eta(v)$ represent the wind condition, $\eta(v)$ denotes the power curve, and c and k correspond to the scale and shape parameters of the Weibull distribution.

AEP is calculated as the product of the estimated energy and 8760 h per year, as given in Equation (3).

$$AEP = 8760\ E \tag{3}$$

3.3. Wake Effect Model

The wake effect is defined as the decrease in wind speed and power that occurs after a wind turbine has extracted energy from the incoming wind, posing a major challenge in large wind farms. Minimizing the wake effect is a primary objective in wind farm design, and optimal turbine distribution is a crucial factor in reducing power loss due to this effect [22].

In the case of large wind farms, downstream wind turbines are often affected by multiple upstream wakes that are generated by several upstream turbines. Therefore, the wake effects with the rotor area belonging to the downstream turbine must be considered, as described in [23]. In this study, the wake model is adopted from [7]. The wake radius produced by an upstream wind turbine expands linearly with the downwind distance dy_{ij} [24], as illustrated in Figure 3 and expressed in Equations (4) and (5), where r_w is the radius of wake at the downstream distance dy_{ij}, r_i is the upstream rotor radius, and k denotes the wake expansion parameter dependent on hub height z and surface roughness length z_0.

$$r_w = r_i + kdy_{ij} \tag{4}$$

$$k = \frac{0.5}{\ln z/z_0} \tag{5}$$

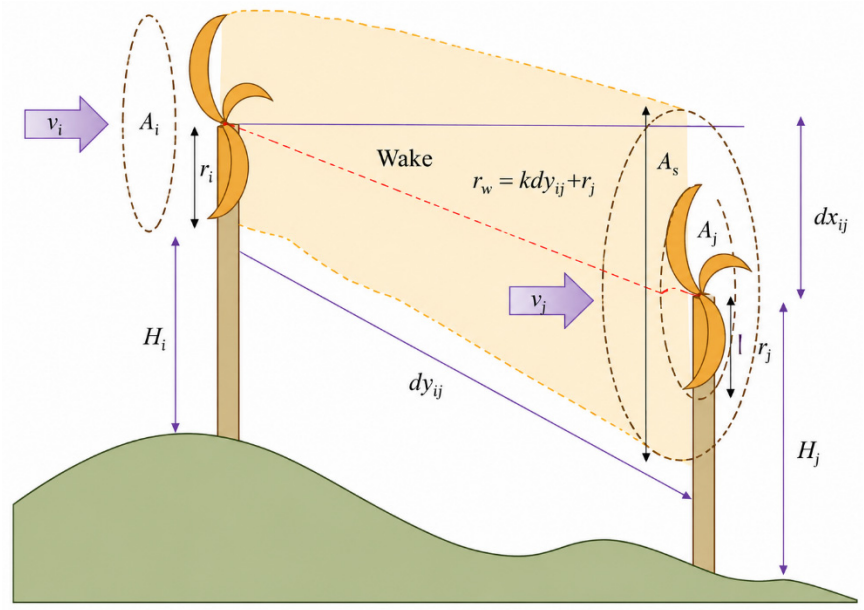


Figure 3. Schematic representation of the wake model, adapted from [7].

Wake overlap area A_s in wind farms between turbines located upstream and downstream can be determined using Equation (6), and the calculation of these wake effects is based on factors such as rotor diameter, wind direction, and Δh, where Δh is the change in hub height. In this study, no variation in hub height is considered, as all turbines are assumed to operate at the same hub height.

$$A_s = {r_w}^2 \cos^{-1}\left(\frac{{dx_{ij}}^2+{r_w}^2+\Delta h^2-{r_j}^2}{2r_w\sqrt{\Delta h^2+{dx_{ij}}^2}}\right) + {r_j}^2 \cos^{-1}\left(\frac{{dx_{ij}}^2+{r_j}^2+\Delta h^2-{r_w}^2}{2r_j\sqrt{\Delta h^2+{dx_{ij}}^2}}\right) - r_w\sqrt{\Delta h^2+{dy_{ij}}^2}.\sin\left(\cos^{-1}\frac{{dx_{ij}}^2+{r_w}^2+\Delta h^2-{r_j}^2}{2r_w\sqrt{\Delta h^2+{dx_{ij}}^2}}\right) \quad (6)$$

The relative locations of upstream and downstream wind turbines change with variations in wind direction θ. Assume that two turbines are defined by coordinates (x_i,y_i) and (x_j, y_j). As the wind direction changes, the relative locations of these turbines are adjusted. The transformed coordinates of each turbine are given in Equation (7), while (dx_{ij},dy_{ij}) in Equation (8) represent the streamwise and lateral distances between the two turbines [25].

$$\begin{bmatrix} x_i' \\ y_i' \end{bmatrix} = \begin{bmatrix} \cos\theta & -sin\theta \\ \sin\theta & \cos\theta \end{bmatrix} \begin{bmatrix} x_i \\ y_i \end{bmatrix} \quad (7)$$

$$dx_{ij} = x_i' - x_j' dy_{ij} = y_i' - y_j' \quad (8)$$

A downstream turbine is influenced by an upstream turbine when the relative streamwise and lateral distances meet the conditions specified in Equation (9).

$$dx_{ij} < 0 \;\&\; \left|dx_{ij}\right| - \frac{D_j}{2} < \frac{D_{wake,ij}}{2} \quad (9)$$

where the wake diameter is expressed as given in Equation (10).

$$D_{wake,ij} = 2\left(k\, dy_{ij} + r_j\right) \quad (10)$$

The wind speed experienced by the downstream turbine v_j decreases as a result of the wake generated by the upstream turbine, as given in Equation (11), where C_T represents the thrust coefficient.

$$v'_j = v_j \left[1 - \sum_{i=1}^{n} \left(1 - \sqrt{1 - C_T}\right) \left(\frac{r_i}{r_i + k\, dy_{ij}} \right)^2 \frac{A_s}{A_j} \right] \tag{11}$$

4. Optimization Algorithm

This section describes the optimization algorithm used to solve the WFLO problem. Due to the nonlinear and complex nature of wind farm layout optimization, metaheuristic algorithms are widely adopted. In this study, the MECPO algorithm is employed due to its enhanced exploration capability and effectiveness in handling constrained optimization problems. The section details the main mechanisms of the algorithm, including initialization, ionization, electron exchange, and interaction processes. Additionally, a double-stage optimization strategy is introduced, combining grid-based optimization with coordinate-based refinement to improve convergence and solution quality.

4.1. MECPO Algorithm

Metaheuristic algorithms are widely used to solve complex optimization problems such as WFLO, where traditional methods often struggle due to nonlinearity, constraints, and large search spaces. One of these algorithms is the electric charged particle optimization (ECPO) algorithm [26], which is inspired by physical interactions between charged particles. In ECPO, candidate solutions are modeled as electric charged particles that interact with each other based on attraction and repulsion principles. These interactions guide the search process toward optimal solutions.

Despite its effectiveness [27,28], the original ECPO algorithm suffers from a limited exploration capability, particularly when applied to coordinate-based WFLO problems. Due to the presence of multiple constraints and a continuous search space, ECPO tends to converge prematurely and may become trapped in local optima. To overcome this limitation, a modified version, MECPO, is proposed. The MECPO algorithm enhances the exploration mechanism of ECPO by incorporating two additional processes inspired by chemical reactions, namely, ionization and electron exchange. These processes introduce new candidate solutions and increase the diversity of the population, allowing the algorithm to explore a wider search space [7]. The intricacies of this modification are elucidated in Figure 4, providing a visual representation of the enhanced MECPO process. Therefore, the MECPO algorithm is selected in this study due to its enhanced exploration capability and its effectiveness in handling constrained and nonlinear WFLO problems, making it suitable for the proposed double-stage optimization framework. In the proposed WFLO framework, MECPO is used as the main search engine to update candidate layouts iteratively. The ionization and electron exchange stages mainly improve exploration by increasing solution diversity, while the interaction stage improves exploitation by guiding candidate solutions toward the best-performing layout. Therefore, MECPO provides a balance between global search and local improvement, which is important for constrained wind farm layout optimization.

The flowchart of the MECPO algorithm is illustrated in Figure 5, while the detailed process of MECPO is described in the following steps:

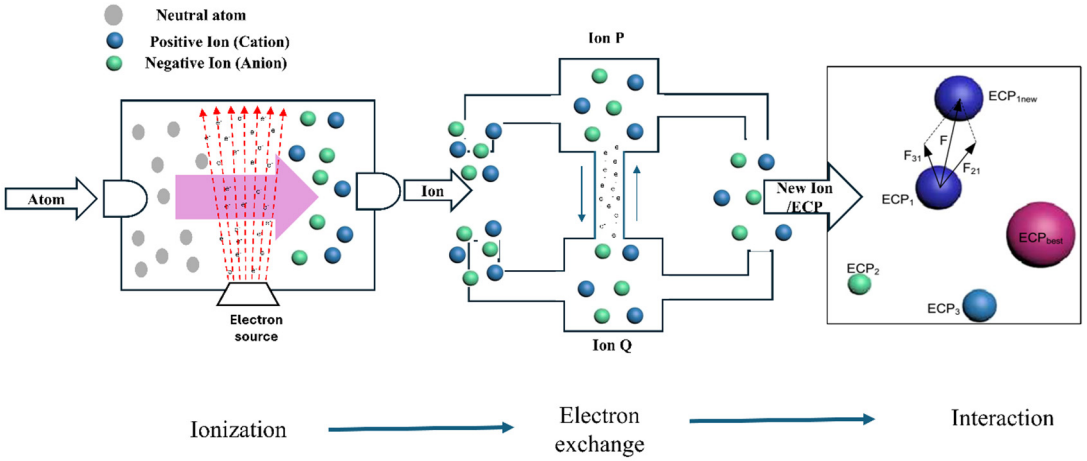


Figure 4. Visual representation of the enhanced MECPO process.

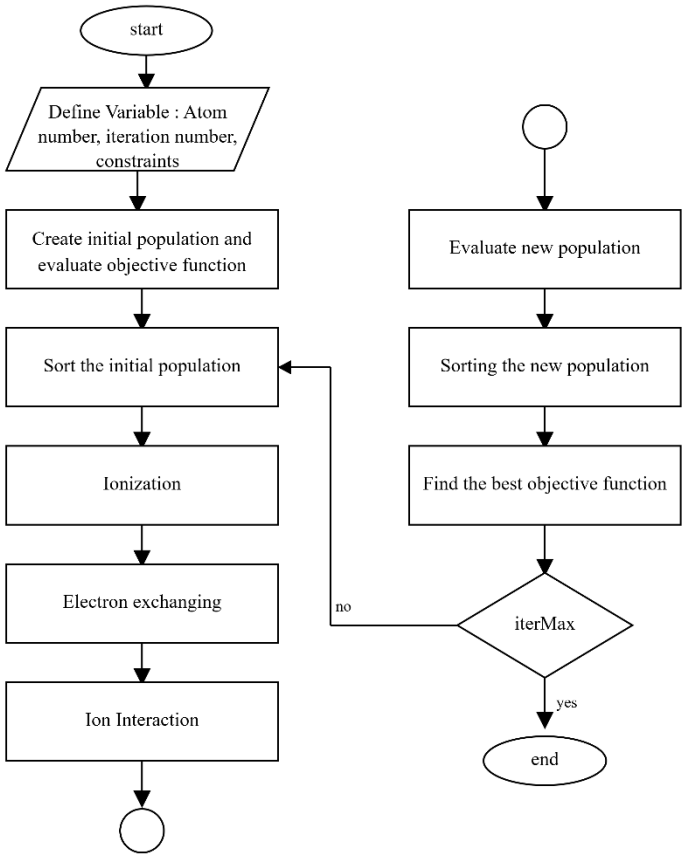


Figure 5. MECPO flowchart.

Initialization: The initialization step begins by generating a population of candidate solutions randomly within the search space. In the MECPO algorithm, each candidate solution is represented as an atom. After generating the initial population, each atom is evaluated using the objective function to measure its performance. Following the evaluation process, the population is sorted according to the objective function values in order to identify the best-performing solution.

Ionization: Once the initial population of atoms is generated, the ionization process is applied to enhance the diversity of the candidate solutions. In this step, each atom is transformed into an ion by modifying its internal structure, which is represented by a

set of decision variables referred to as electrons. Each atom can be expressed as a vector of electrons:

$$x_i = [x_1 + x_2 + \cdots + x_M] \tag{12}$$

where M represents the number of electrons in each atom. During the ionization process, each electron is perturbed by adding a random value drawn from a normal distribution. This modification is defined as:

$$x_i' = x_i + p \tag{13}$$

This operation introduces controlled variations in the atoms, transforming them into ions and enabling the algorithm to explore new regions within the search space. Consequently, the ionization process improves the exploration capability and reduces the risk of premature convergence.

Electron exchange: This mechanism draws its idea from redox reactions, where electrons move between ions, leading to the formation of new ions and consequently widening the search space. Consider two ions, P and Q, where each one is described by a vector of electrons $[x_1 + x_2 + \cdots + x_M]$. The variable M denotes the total number of electrons in each ion. At the start, two ions are selected randomly from the population, after which the electron exchange procedure is applied as follows:

- A random integer k is generated such that $1 \leq k \leq M - 1$, which determines how the electrons are split between the two ions.
- The first k electrons from ion P are combined with the remaining (M − k) electrons taken from ion Q to construct a new ion.
- In a similar manner, another ion is formed by taking the first k electrons from ion Q and merging them with the remaining electrons from ion P.
- These newly constructed ions are then treated as candidate solutions and passed forward to the subsequent stages of the ECPO algorithm.

Interaction: During the interaction stage, each ECP simultaneously interacts with both the best-performing ECP and another ECP, leading to the generation of an updated solution. This interaction is mathematically described as:

$$ECP_{new}^{t+1} = {ECP_1}^t + \beta\, x\, \left(ECP_{best}^t - {ECP_1}^t\right) + \beta\, x\, \left({ECP_1}^t - {ECP_2}^t\right) \tag{14}$$

where β is a stochastic control parameter generated using a normal distribution, t denotes the current iteration, and $t + 1$ denotes the next iteration.

Bound check: After the interaction stage, the newly generated electric charged particles are examined to ensure that their positions remain within the predefined search boundaries. Any particle that violates the search limits is adjusted and projected back into the feasible search space.

4.2. Double-Stage MECPO-Based Optimization

This section presents the proposed double-stage optimization framework for wind farm layout design. The approach integrates both grid-based and coordinate-based models to exploit their respective advantages. This integration is adopted to balance the trade-off between computational efficiency and optimization flexibility. Specifically, the grid-based stage provides a structured and computationally efficient initial layout, while the coordinate-based stage enables flexible local optimization to improve turbine positioning and reduce wake interactions, as shown in Figure 6.

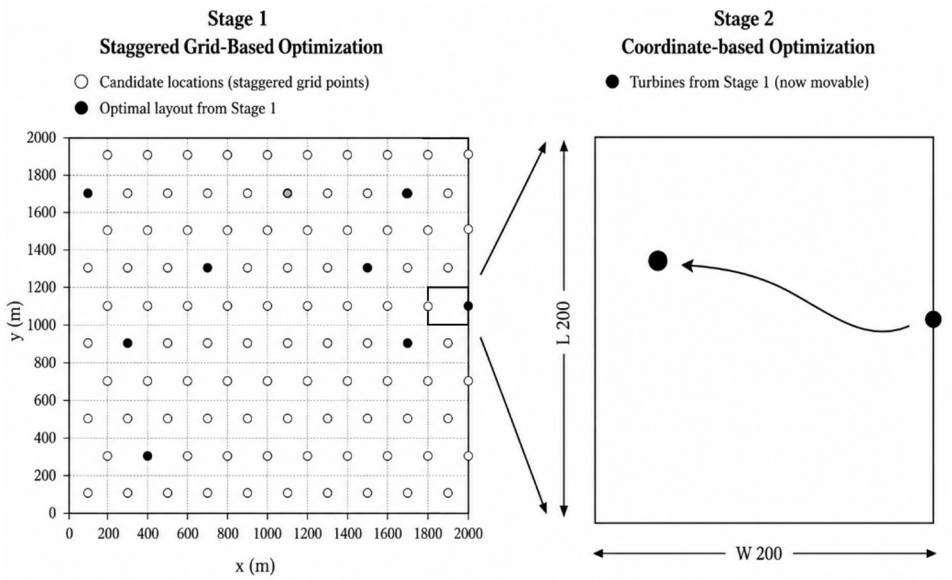


Figure 6. Schematic illustration of wind turbine position refinement.

In the first stage, structured grid-based optimization is performed using a staggered layout to determine initial turbine locations. This configuration ensures a well-distributed spatial arrangement and reduces direct turbine alignment, thereby mitigating wake interactions. In the second stage, the turbine positions obtained from the first stage are further optimized locally using a coordinate-based representation. The main difference between the double-stage with a staggered grid and double-stage with a square grid approaches lies in the spatial arrangement used during Stage 1. In the staggered grid configuration, alternate rows are shifted to reduce direct turbine alignment and wake overlap, whereas the square grid employs aligned turbine rows with uniform spacing. Both approaches use the same coordinate-based local refinement in Stage 2. This local optimization allows for controlled adjustments of turbine positions within predefined grid cells, aiming to reduce wake interactions and improve energy capture.

The main steps of the proposed double-stage optimization framework are summarized as follows:

1. The wind farm area is discretized into grid cells, and candidate turbine locations are generated using a structured staggered grid configuration to reduce direct turbine alignment and improve spatial distribution.
2. Grid-based optimization is performed to determine the optimal turbine layout from the candidate positions.
3. The resulting layout is used as the initial solution for Stage 2.
4. In Stage 2, coordinate-based local optimization is applied, allowing each turbine to move freely within its original grid cell while remaining constrained within its assigned boundaries.
5. The optimization continues in Stage 2 to further improve energy capture and reduce wake effects.

The proposed framework integrates the staggered grid-based and coordinate-based approaches within a unified optimization procedure. The overall workflow of the proposed double-stage optimization framework is illustrated in Figure 7.

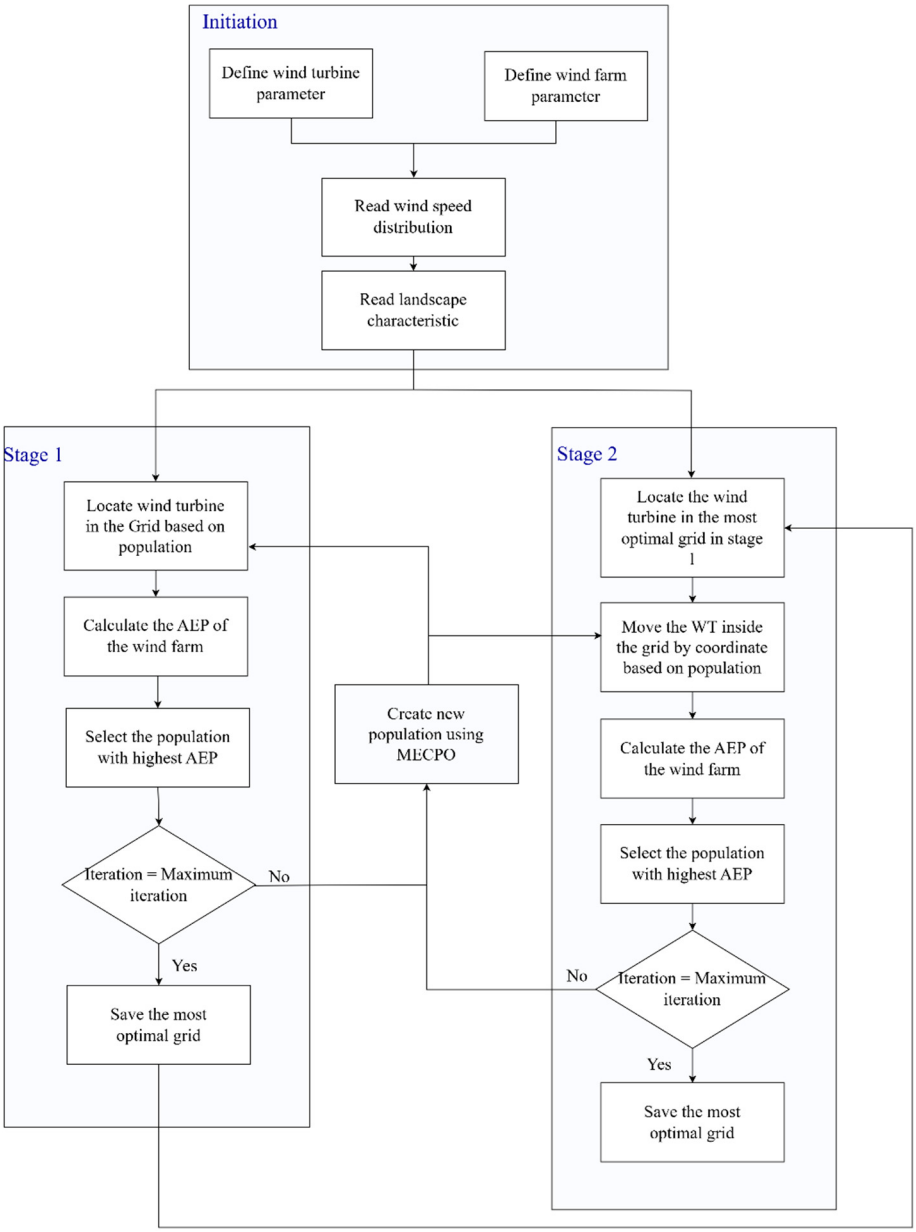


Figure 7. Flowchart of double-stage optimization.

4.3. Staggered Grid-Based Optimization

In Stage 1, the grid-based optimization approach is employed using a structured staggered grid layout to improve spatial distribution and reduce turbine alignment. This configuration is selected due to its near-isotropic spatial characteristics, which provide more uniform turbine spacing compared with the conventional square grid and help reduce directional wake alignment.

Let the wind farm area be discretized into an $m \times n$ grid, yielding $G = \{g_{ij} | i = 1, \ldots, m;\ j = 1, \ldots, n\}$ possible grid cells.

To improve turbine distribution and reduce wake alignment, a staggered grid configuration is adopted. The coordinates of each candidate location are defined as

$$\begin{aligned} x_{i,j} &= jd_x - \tfrac{d_x}{2} + \tfrac{d_x}{2}\delta(i) \\ y_{i,j} &= id_y - \tfrac{d_y}{2} \\ \delta(i) &= \begin{cases} 0, & \text{if } i \text{ odd} \\ 1, & \text{if } i \text{ even} \end{cases} \end{aligned} \tag{15}$$

where i and j denote the row and column indices, respectively; d_x and d_y represent the horizontal and vertical grid spacing; and $\delta(i)$ is the staggering function. In this study, the grid spacing is defined as

$$d_x = dy = 5D$$

where D is the rotor diameter. When the inter-turbine spacing is less than $5D$, strong wake interactions occur, significantly affecting downstream turbines. Therefore, $5D$ is considered a practical design threshold for mitigating wake effects in wind farm layout optimization [29].

The turbine placement is modeled using binary decision variables:

$$z_{ij} = \begin{cases} 1 \text{ if a turbine is placed at grid cell } g_{ij} \\ 0 \qquad\qquad\qquad \text{otherwise} \end{cases} \tag{16}$$

subject to

$$\sum_{i=1}^{m} \sum_{j=1}^{n} z_{ij} = N_{WT} \tag{17}$$

where N_{WT} is the predefined number of wind turbines.

4.4. Coordinate-Based Local Refinement

In Stage 2, the turbine positions obtained from Stage 1 are locally refined within their grid cells. This local refinement strategy is adopted to limit the search space and reduce computational cost, while still allowing for sufficient flexibility to improve turbine positioning. The updated turbine positions are given by

$$x_t = x_t^0 - \frac{d_x}{2} + \delta x_t, y_t = y_t^0 - \frac{d_y}{2} + \delta y_t \tag{18}$$

where x_t^0 and y_t^0 denote the initial turbine coordinates obtained from Stage 1.

The local offsets are constrained within the grid cell:

$$0 \leq \delta x_t \leq d_x, 0 \leq \delta y_t \leq d_y$$

This formulation enables local adjustment of turbine positions while preserving the overall layout structure.

The turbine positions must satisfy the wind farm boundaries:

$$0 \leq x_t \leq W, 0 \leq y_t \leq L$$

The minimum distance between any two turbines is defined as:

$$\sqrt{(x_p - x_q)^2 + (y_p - y_q)^2} \geq 5D, \forall_p \neq q$$

A penalty-based constraint handling mechanism is incorporated into the objective function to penalize infeasible turbine layouts violating the constraints.

5. Results and Discussion

The proposed approach is evaluated on a 2 km × 2 km wind farm in three wind scenarios: single-direction wind conditions, uniform multi-directional wind conditions, and spatially varying wind conditions. The performance is compared with a double-stage approach that employs a square grid layout in the first stage and coordinate-based optimization in the second stage. In addition, three single-stage approaches are considered: a square grid-based approach, a staggered grid-based approach, and a coordinate-based

approach. For each optimization strategy, 10 independent runs are performed. The reported net AEP, gross AEP, and wake loss values are expressed as mean ± standard deviation (SD), while the computational time represents the average execution time over the independent runs. All simulations are conducted on an HP Pavilion 14 laptop equipped with an Intel Core i7-1165G7 (11th Gen) processor, 16 GB of RAM, running Windows 10 Home (64-bit). The objective of the optimization is to maximize AEP. Table 1 summarizes the parameter settings of the MECPO algorithm, while Table 2 presents the specifications of the wind turbines used in this study along with the wind farm data.

Table 1. Parameter settings of MECPO algorithm.

Population size	50
Ion interaction coefficient	5
Ion exchanging coefficient	0.5
Ion ionization coefficient	0.5

Table 2. Wind farm parameters.

Parameter	Description	Value
H	hub height (m)	60
P_{rate}	power rate (kW)	620
D_i	diameter rotor (m)	40
$v_{cut\text{-}in}$	cut-in speed of WT (m/s)	2
v_{rate}	rated speed (m/s)	12.5
$v_{cut\text{-}out}$	cut-out speed of WT (m/s)	18
C_T	thrust coefficient of WT	0.88

The wind turbine parameters and wind farm data are based on [11]. However, the surface roughness length z_0 is adjusted from 0.3 to 0.08 to represent typical farmland terrain conditions, as z_0 values for such terrain commonly range from 0.05 to 0.1 [30]. The number of turbines is set to 20 to ensure a reasonable balance between energy production and wake interaction effects while maintaining a manageable optimization problem size.

5.1. Wind Data

The three investigated wind scenarios are illustrated in Figure 8. These scenarios represent different levels of wind complexity, ranging from a simplified baseline case to more realistic and spatially varying conditions.

1. In this case, a single wind direction is considered, while all other directions are neglected. The wind field is modeled using a Weibull distribution with identical parameters, characterized by a scale parameter of C = 12 m/s.
2. A uniform multi-directional wind distribution is considered using 12 wind directions with equal occurrence probability. All directions share identical Weibull parameters, with a scale parameter C = 12 m/s. This configuration represents a more realistic wind condition compared with the single-direction case while still maintaining uniformity across directions.
3. A uniform multi-directional wind distribution is adopted using 12 equally probable wind directions. To introduce spatial variability, a prescribed linear gradient is applied to the Weibull scale parameter C along the Y-direction, resulting in a gradual increase in wind intensity across the wind farm of up to 10%. This scenario represents a more complex wind environment and is used to evaluate the robustness of the proposed optimization framework under spatially varying conditions.

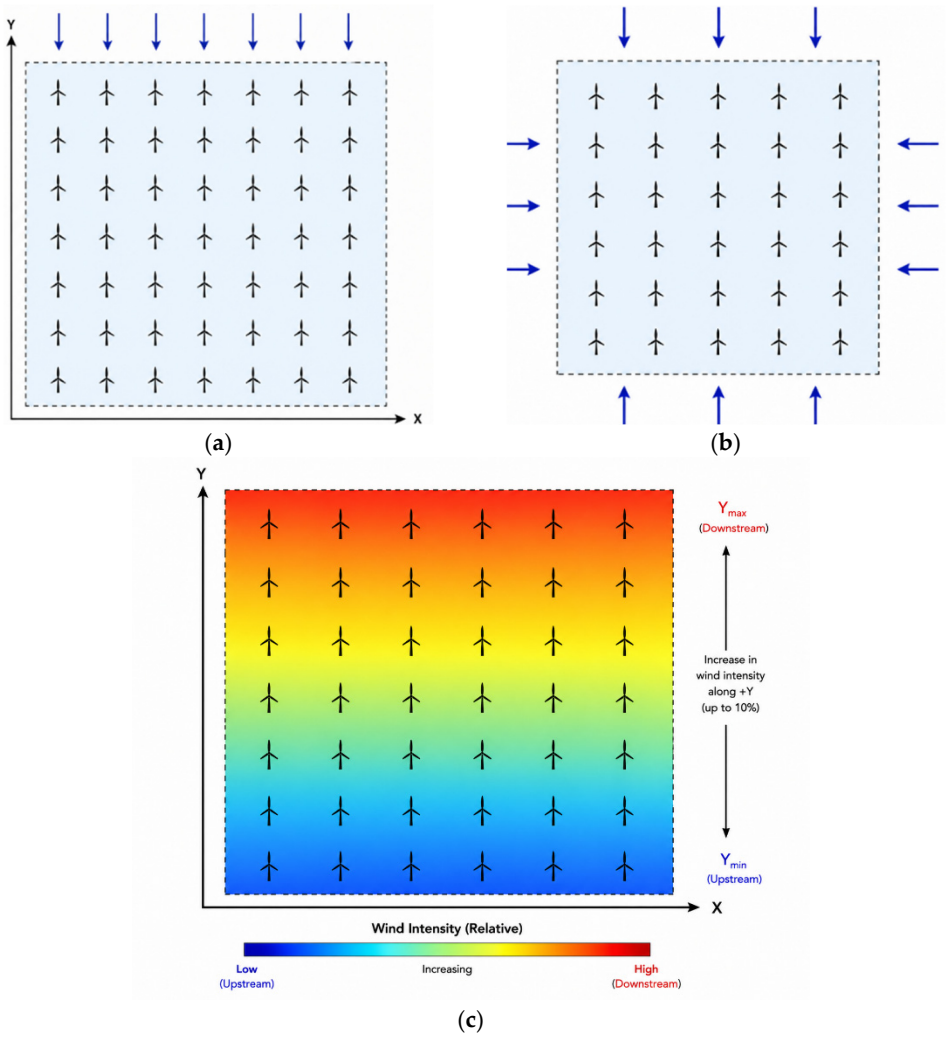


Figure 8. Wind scenarios: (**a**) single-direction; (**b**) uniform multi-directional; and (**c**) spatially varying wind conditions.

5.2. Single-Direction Wind Condition

Under single-direction wind conditions, the proposed double-stage optimization is implemented and evaluated and is compared with a double-stage approach that employs a square grid layout, as well as three single-stage approaches. Table 3 summarizes the performance of the different layout strategies in terms of AEP, wake effect, and computational time, while Figures 9 and 10 illustrate the resulting wind farm layouts across the two optimization stages. In addition, Figure 11 presents the convergence behavior of net AEP for both double-stage approaches.

Table 3. Performance comparison of different WFLO strategies under single-direction wind conditions.

Approach	Net AEP (GWh)		Wake Loss (%)		Gross AEP (GWh)	Computational Time (s)	Iterations
	Mean	SD	Mean	SD			
Double-stage (staggered grid)	80.79	0.01	0.68	0.02	81.3478	184.11	100 + 100
Double-stage (square grid)	80.70	0.06	0.79	0.08		189.83	100 + 100
Single-stage (staggered grid)	80.69	0.00	0.806	0.00		188.92	200
Single-stage (square grid)	80.61	0.08	0.89	0.10		189.51	200
Single-stage (coordinate-based)	80.76	0.094	0.71	0.11		1726.03	200

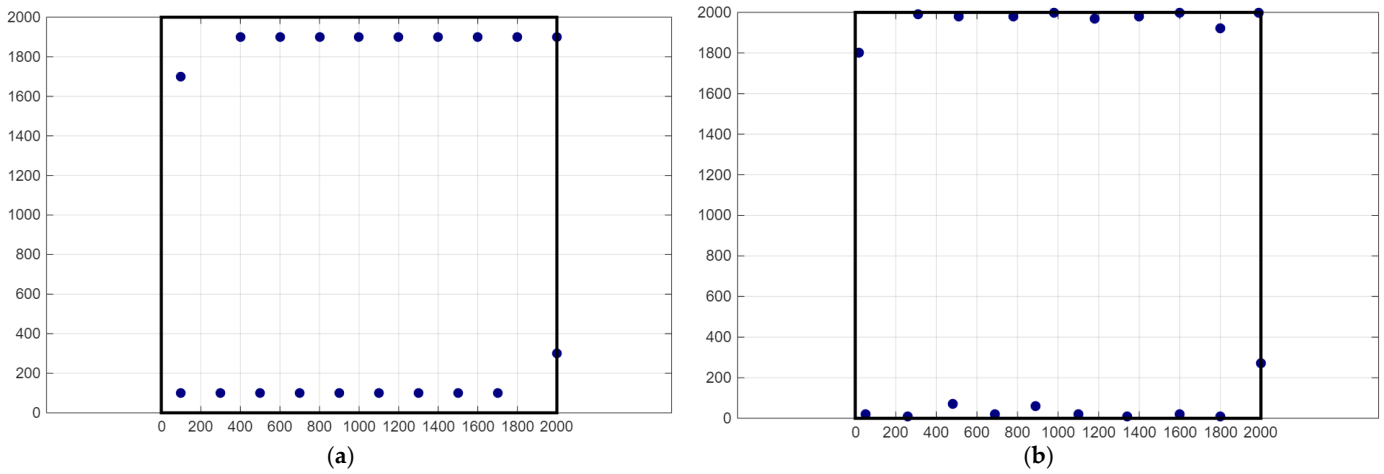


Figure 9. Optimal wind farm layout for the double-stage optimization with a staggered grid under single-direction wind conditions: (**a**) Stage 1; (**b**) Stage 2.

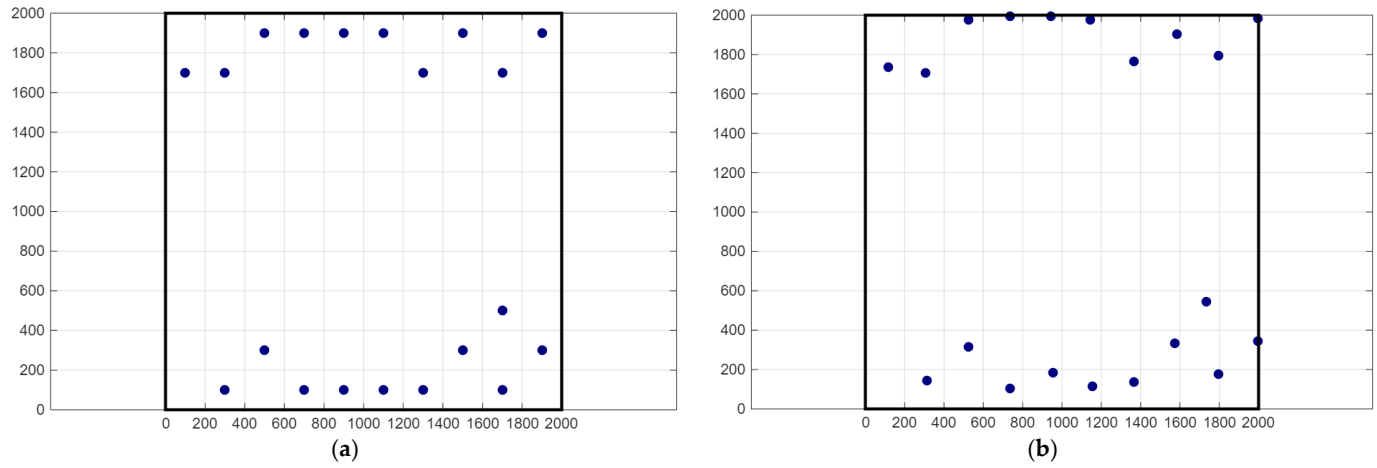


Figure 10. Optimal wind farm layout for the double-stage optimization with a square grid under single-direction wind conditions: (**a**) Stage 1; (**b**) Stage 2.

Under single-direction wind conditions, the optimization process is primarily governed by turbine alignment along the dominant wind direction. In this context, the quality of the initial layout plays a crucial role in determining both the convergence behavior and the final performance. As shown in Figures 9 and 10, the proposed double-stage optimization with a staggered grid results in a more evenly distributed turbine layout compared with the square grid, which exhibits a higher degree of turbine alignment. This initial staggered distribution reduces direct wake overlap between downstream turbines, leading to a more balanced flow field across the wind farm. Consequently, the optimization process starts from a more favorable initial layout.

The convergence behavior illustrated in Figure 11 indicates that the double-stage optimization with a staggered grid starts closer to the final solution and requires fewer adjustments during the second stage. This suggests that the search space is more effectively explored from the outset, reducing the need for extensive turbine repositioning. In contrast, the double-stage optimization with a square grid starts from a less favorable configuration, in which turbine alignment along the wind direction leads to increased wake interactions and energy losses. As a result, the optimization process requires more iterations to redistribute turbines and mitigate these wake effects.

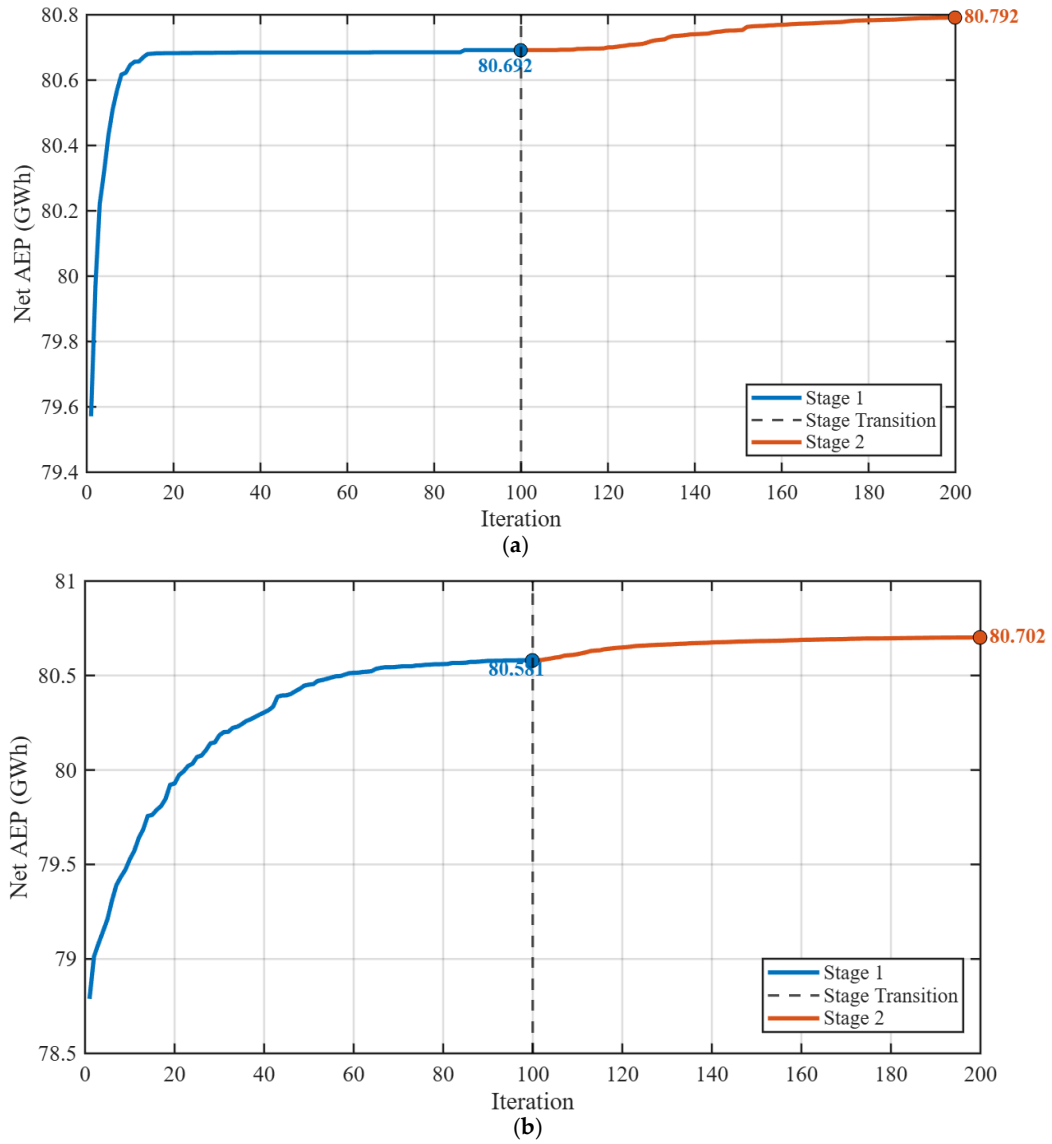


Figure 11. Convergence curve of net AEP for the double-stage optimization under single-direction wind conditions: (**a**) staggered grid; (**b**) square grid.

Furthermore, the improved initial spacing in the staggered configuration contributes to faster convergence and enhanced AEP, as the algorithm focuses on fine-tuning turbine positions rather than correcting large-scale layout inefficiencies.

The results in Table 3 show that the double-stage optimization with a staggered grid achieves a slightly higher net AEP of 80.79 GWh, compared with 80.70 GWh for the same approach using a square grid. This improvement is accompanied by a reduction in wake losses from 0.79% to 0.68%, indicating more effective initial turbine spacing. Interestingly, the single-stage staggered grid configuration achieves a net AEP very close to that of the double-stage approach with a square grid. This can be attributed to the offset arrangement of turbines in the staggered layout, which reduces direct downstream wake interactions. In contrast, the square grid introduces aligned turbine rows that intensify wake effects, which cannot be fully mitigated by the local optimization stage. As observed in Table 3, the gross AEP remains constant across all approaches, as it depends on the wind resource and turbine characteristics rather than turbine positioning. Therefore, the observed differences in performance are mainly reflected in the net AEP due to variations in wake interactions.

Under single-direction wind conditions, the performance of single-stage approaches is relatively close to that of the double-stage approaches, as wake interactions are easier

to manage when wind originates from a dominant direction. The coordinate-based approach achieves a comparable net AEP of 80.76 GWh, demonstrating its capability to reach near-optimal solutions. However, this performance comes at a significantly higher computational cost, requiring 1726.03 s compared with approximately 189 s for the double-stage approaches. This highlights a clear trade-off between solution quality and computational efficiency, as the expanded continuous search space increases the computational burden. This observation is consistent with previous studies [7,9], which reported that grid-based approaches offer lower computational cost but limited flexibility, while coordinate-based methods achieve higher solution quality at the expense of increased computational effort.

Overall, although all approaches yield similar energy performance under single-direction wind conditions, the double-stage approach, particularly with a staggered grid, provides a more favorable balance between performance and computational cost, making it a more practical and time-efficient solution for wind farm layout optimization.

This finding is also consistent with hybrid optimization frameworks reported in the literature [20], where structured initialization improves convergence efficiency and overall performance.

5.3. Uniform Multi-Directional Wind Conditions

Under uniform multi-directional wind conditions, the proposed approach is further assessed against a double-stage approach based on a square grid and three single-stage approaches. Table 4 presents the performance of the layout strategies in terms of AEP, wake effect, and computational time. The resulting wind farm layouts are shown in Figures 12 and 13, while Figure 14 illustrates the convergence behavior of net AEP for the double-stage approaches.

Table 4. Performance comparison of different WFLO strategies under uniform multi-directional wind conditions.

Approach	Net AEP (GWh)		Wake Loss (%)		Gross AEP (GWh)	Computational Time (s)	Iterations
	Mean	SD	Mean	SD			
Double-stage (staggered grid)	79.762	0.027	1.949	0.033	81.3478	190.05	100 + 100
Double-stage (square grid)	79.669	0.043	2.064	0.053		192.58	100 + 100
Single-stage (staggered grid)	79.529	0.023	2.235	0.028		189.10	200
Single-stage (square grid)	79.526	0.024	2.238	0.029		192.18	200
Single-stage (coordinate-based)	79.645	0.049	2.092	0.060		1400.61	200

Under uniform multi-directional wind conditions, the wind farm layout optimization problem becomes more complex due to the superposition of wake effects across multiple inflow directions and the absence of a dominant energy-weighted wind sector. Consequently, performance is no longer governed by directional alignment but rather by achieving a more uniformly distributed turbine layout that minimizes cumulative wake interactions from all directions.

As illustrated in Figures 12 and 13, the geometric arrangement of turbines differs significantly between the double-stage optimization with a staggered grid and that based on a conventional square grid. The staggered layout provides a more directionally uniform spatial distribution, reducing directional dependency compared with the square grid configuration. In contrast, the double-stage optimization with a square grid follows an orthogonal structure, which introduces directional dependency and leads to non-uniform effective spacing under oblique wind conditions.

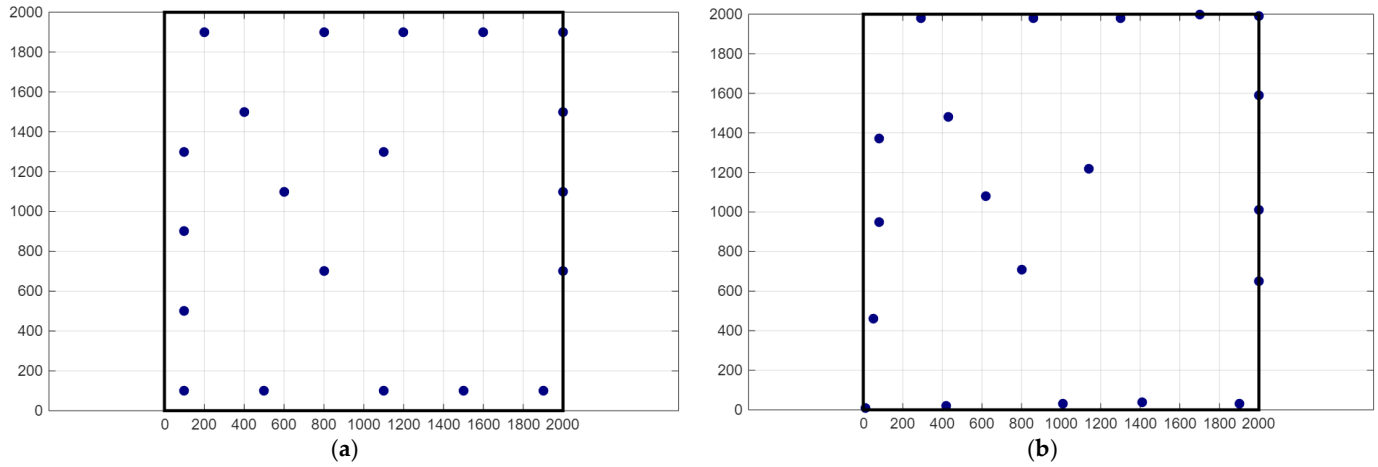


Figure 12. Optimal wind farm layout for the double-stage optimization with a staggered grid under uniform multi-directional wind conditions: (**a**) Stage 1; (**b**) Stage 2.

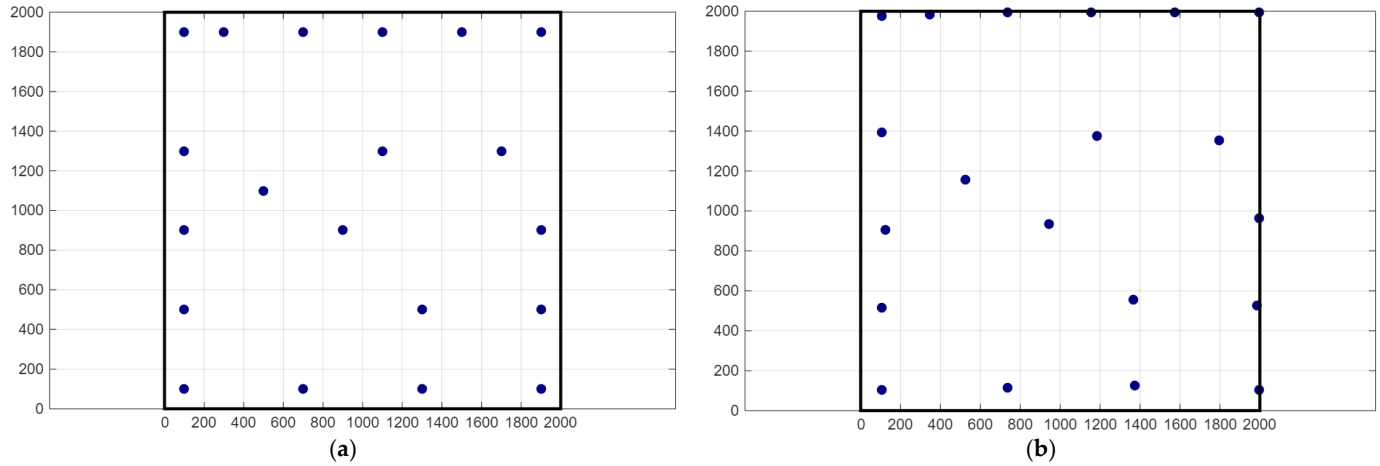


Figure 13. Optimal wind farm layout for the double-stage optimization with a square grid under uniform multi-directional wind conditions: (**a**) Stage 1; (**b**) Stage 2.

Figure 14 shows that the staggered grid configuration achieved better performance than the square grid configuration during both optimization stages. The staggered grid case started with a higher net AEP at the end of Stage 1 and continued to achieve additional improvement during Stage 2, reaching the highest final net AEP value. In contrast, the square grid configuration exhibited a similar convergence trend but with a lower improvement rate and a lower final net AEP. This indicates that the staggered geometric arrangement provides a more effective initial layout for the coordinate-based local optimization stage.

The results in Table 4 further support these observations. Compared with single-directional wind conditions, a decrease in net AEP was observed, accompanied by an increase in energy loss due to wake effects. This indicates a higher level of complexity in wake interactions when winds blow from multiple directions. The double-stage optimization with a staggered grid achieves the highest net AEP of 79.76 GWh, compared with 79.66 GWh for the double-stage optimization with a square grid. This improvement can be attributed to increased lateral spacing between turbines, which enhances wake recovery and reduces cumulative wake interactions. This behavior is consistent with previous findings [13], where isotropic or hexagonal-like layouts were shown to reduce wake interactions under multi-directional wind conditions. Although the absolute improvement in net AEP is relatively small, it shows that the staggered initialization provides a more

effective starting layout for reducing cumulative wake interactions under multi-directional wind conditions.

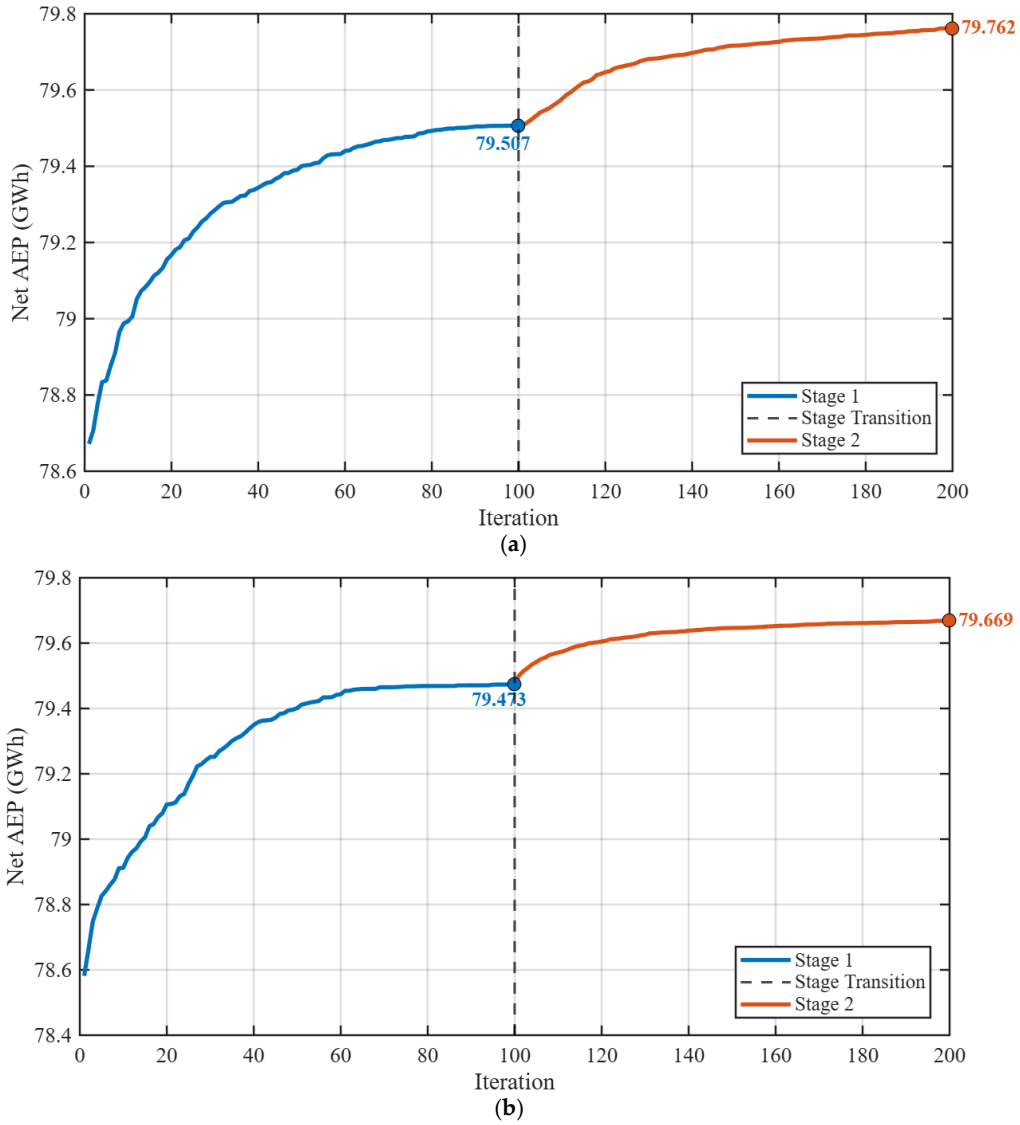


Figure 14. Convergence curve of net AEP for the double-stage optimization under uniform multi-directional wind conditions: (**a**) staggered grid; (**b**) square grid.

Among the single-stage approaches, the coordinate-based method achieves the best performance, with a net AEP of 79.64 GWh and a wake loss of 2.092%. This indicates that the coordinate-based approach can produce competitive layouts by exploring a continuous solution space. However, this advantage comes with a much higher computational cost, requiring 1400.61 s compared with 190.05 s and 192.58 s for the double-stage staggered and square grid approaches, respectively. Similar observations have been reported in [15,18], where the increased flexibility of coordinate-based approaches leads to higher computational complexity in nonlinear wake-dominated optimization problems. This indicates that increased flexibility expands the search space and leads to higher computational demand. In contrast, single-stage grid-based approaches exhibit lower performance overall, with only minor differences between staggered and square configurations. Overall, these results align with the general trend reported in the literature, where hybrid approaches outperform grid-based ones by balancing structure and flexibility [20].

5.4. Spatially Varying Wind Conditions

For spatially varying wind conditions, the performance of the proposed double-stage optimization approach is analyzed and compared with a square grid counterpart and three single-stage approaches. Table 5 reports the results in terms of AEP, wake effect, and computational time. Figures 15 and 16 present the optimized wind farm layouts, while Figure 17 shows the convergence behavior of net AEP for the double-stage approaches.

Table 5. Performance comparison of different WFLO strategies under spatially varying wind conditions.

Approach	Net AEP (GWh)		Wake Loss (%)		Gross AEP (GWh)		Computational Time (s)	Iterations
	Mean	SD	Mean	SD	Mean	SD		
Double-stage (staggered grid)	83.38	0.03	2.22	0.19	85.28	0.15	194.74	100 + 100
Double-stage (square grid)	83.29	0.04	2.24	0.08	85.20	0.05	196.54	100 + 100
Single-stage (staggered grid)	83.04	0.02	2.70	0.12	85.35	0.09	193.09	200
Single-stage (square grid)	83.02	0.02	2.57	0.13	85.21	0.10	183.59	200
Single-stage (coordinate-based)	83.08	0.06	2.35	0.06	85.09	0.09	2173.11	200

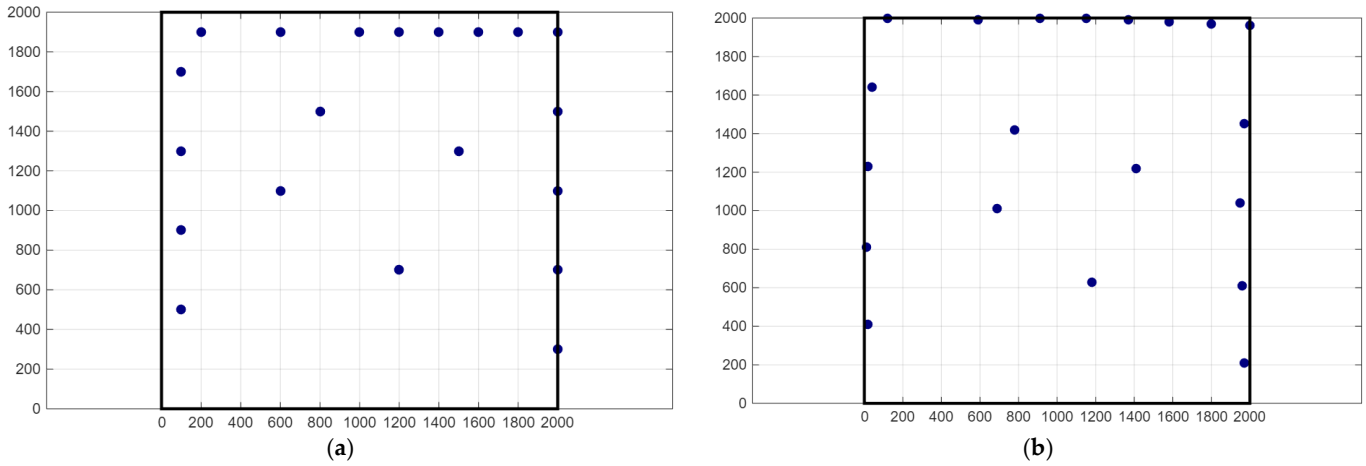


Figure 15. Optimal wind farm layout for the double-stage optimization with a staggered grid under spatially varying wind conditions: (**a**) Stage 1; (**b**) Stage 2.

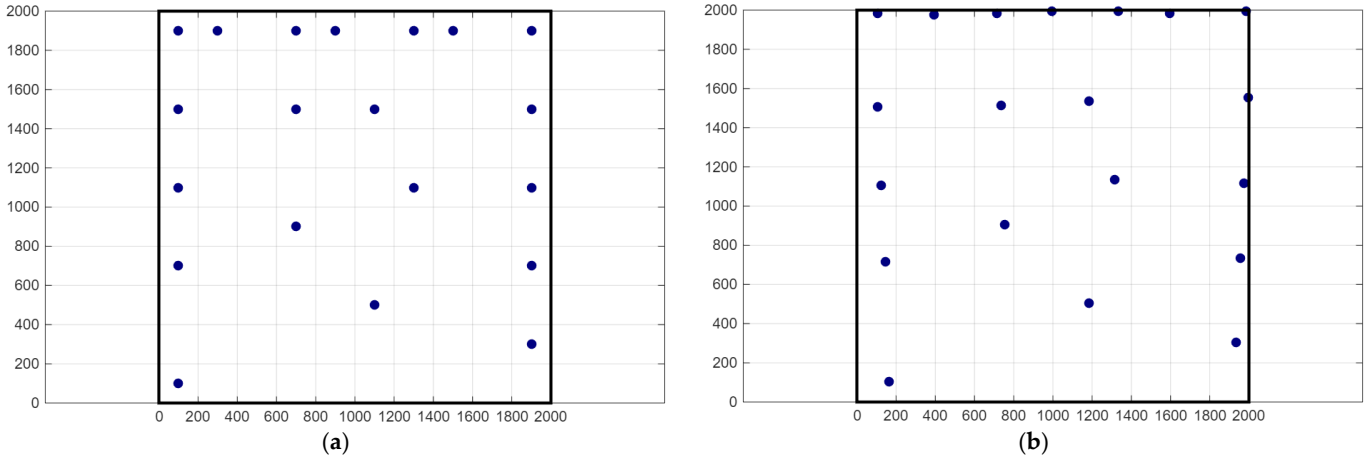


Figure 16. Optimal wind farm layout for the double-stage optimization with a square grid under spatially varying wind conditions: (**a**) Stage 1; (**b**) Stage 2.

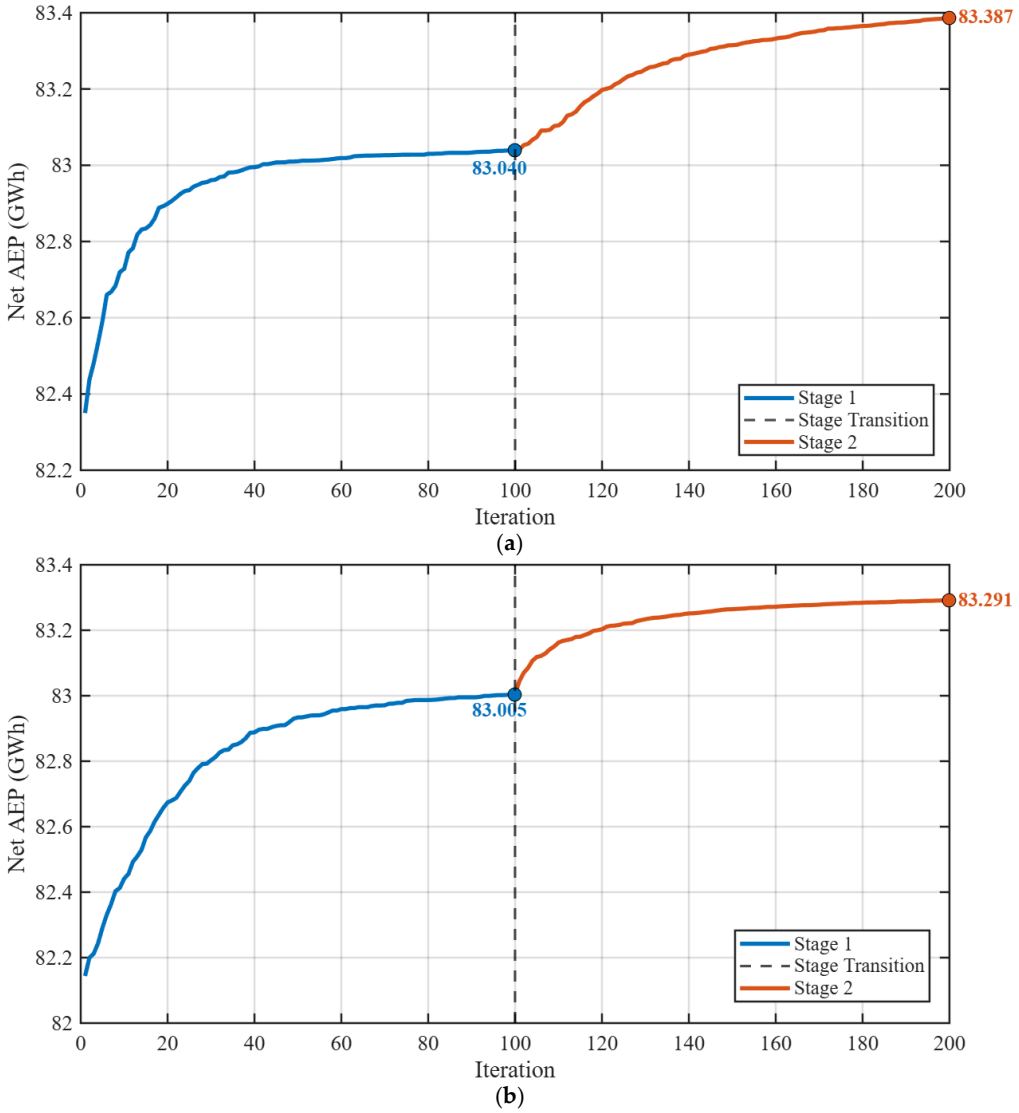


Figure 17. Convergence curve of net AEP for the double-stage optimization under spatially varying wind conditions: (**a**) staggered grid; (**b**) square grid.

Under spatially varying wind conditions, the optimization problem becomes significantly more complex due to the combined influence of multi-directional wind distribution and spatial variation in wind intensity. The imposed gradient in the Weibull scale parameter along the Y-direction encourages turbines to shift toward higher wind regions, while wake interactions impose constraints on turbine spacing. As a result, the optimization process is governed by competing mechanisms between maximizing wind resource and minimizing wake losses. This behavior reflects the nonlinear nature of WFLO under spatially varying wind conditions, as highlighted in previous studies [15].

As shown in Figures 15 and 16, both double-stage approaches result in a noticeable redistribution of turbines during the second stage. In the case of a staggered grid configuration, turbines gradually shift toward higher wind potential regions while maintaining a relatively uniform spatial distribution, thereby avoiding excessive clustering. In contrast, in the square grid configuration, the layout exhibits a stronger tendency for turbine concentration in the upper region of the domain, indicating more aggressive exploitation of high-wind regions. This difference suggests that the staggered configuration provides a more flexible spatial structure, allowing turbines to follow the wind gradient without significantly compromising inter-turbine spacing.

The convergence curves in Figure 17 further highlight the impact of the grid configuration. The double-stage approach with a staggered grid achieves a higher net AEP during Stage 1, indicating that the initial layout is already closer to an effective solution. In contrast, the double-stage approach with a square grid starts from a slightly less favorable configuration and requires more adjustments to improve performance. During Stage 2, both approaches show improvement; however, the staggered configuration benefits from a refinement process, while the square grid undergoes more corrective adjustments to compensate for earlier spatial inefficiencies. This indicates that the initial lattice structure plays a crucial role in guiding the optimization trajectory and influencing convergence efficiency.

In contrast, the staggered grid configuration provides a more efficient spatial distribution, enabling controlled exploitation of high-energy regions while maintaining sufficient turbine spacing. This leads to reduced wake losses and improved overall performance. Furthermore, the convergence behavior indicates that the initial lattice structure significantly influences the solution trajectory. The staggered configuration facilitates efficient refinement, whereas the square grid requires corrective adjustments to overcome early-stage spatial inefficiencies.

These findings highlight the importance of considering both geometric arrangement and spatial wind variability in wind farm layout optimization, as well as the nonlinear relationship between gross and net energy production.

The results in Table 5 indicate that the double-stage approach with a staggered grid provides the best overall performance under spatially varying wind conditions. The staggered grid configuration achieves the highest gross AEP of 85.28 GWh while also maintaining slightly lower wake losses of 2.22% compared with the square-grid configuration. As a result, the staggered grid approach produces the highest net AEP of 83.39 GWh. In contrast, the double-stage approach with a square grid achieves a slightly lower gross AEP of 85.20 GWh and slightly higher wake losses of 2.24%, resulting in a lower net AEP of 83.29 GWh.

The coordinate-based approach achieves a net AEP of 83.08 GWh, similar to single-stage approaches, indicating no significant performance advantage. However, it exhibits the lowest wake losses among the single-stage approaches, along with the lowest gross AEP of 85.09 GWh. This observation is consistent with previous studies describing coordinate-based formulations as more flexible in turbine placement [14]. As a result, the reduction in wake interactions does not translate into higher overall energy production. It is also observed that the computational cost of the coordinate-based approach increases under spatially varying wind conditions. Compared with the single-direction and uniform multi-directional cases, the execution time becomes higher when spatial variation in wind resource distribution across the wind farm is introduced.

This increase is not primarily due to the number of wind directions but rather to the added complexity of spatial wind variability. In the presence of a wind gradient, the optimizer must simultaneously balance multiple competing factors, including exploiting high-wind regions, maintaining adequate turbine spacing, and minimizing wake interactions. Overall, these findings are consistent with the general trends reported in the literature.

6. Conclusions

This study presents a double-stage optimization framework for WFLO, combining staggered grid-based and coordinate-based optimization approaches, in which structured grid-based optimization is first employed to generate an efficient initial turbine layout, followed by coordinate-based refinement to further enhance turbine positioning and mitigate wake interactions. The main findings of this study can be summarized as follows:

- The proposed double-stage approach with a staggered grid achieved the highest net AEP across all investigated wind scenarios. Compared with the coordinate-based approach, it improved net AEP by up to 0.36%, reduced wake losses by up to 6.84%, and decreased computational time by up to 90%.
- Under single-direction wind conditions, the proposed approach achieved a net AEP of 80.79 GWh, with reduced wake losses of 0.68%, outperforming the square-grid-based approach.
- Under uniform multi-directional wind conditions, the staggered grid configuration consistently reduced wake losses and improved spatial balance compared with the square grid configuration.
- Under spatially varying wind conditions, the proposed approach achieved the highest net AEP of 83.38 GWh, with a reduction in wake losses of 2.22% compared with other methods, while reducing computational time by more than 90%.
- The results confirm that the initial spatial configuration has an impact on optimization performance, where the staggered grid provides a more effective and stable starting point.
- The proposed framework achieves a better balance between energy performance and computational cost compared with both grid-based and coordinate-based single-stage approaches.

From a practical perspective, the proposed framework is particularly suitable for early-stage wind farm design and large-scale applications, where computational efficiency is critical. It can support engineering decision making by enabling the evaluation of alternative turbine layouts under different wind conditions prior to implementation. Despite these promising results, this study is subject to certain limitations. The analysis is based on simulated wind conditions and a fixed set of model parameters. Future work may extend the proposed framework to multi-objective optimization, incorporating additional factors such as cost, environmental impact, and real wind data.

Author Contributions: Conceptualization, F.S.A.-O.; methodology, F.S.A.-O.; software, F.S.A.-O.; validation, F.S.A.-O., M.A.M.R., Y.A.A.-T. and M.A.-Z.; formal analysis, F.S.A.-O.; investigation, F.S.A.-O. and M.A.-Z.; resources, F.S.A.-O.; data curation, F.S.A.-O.; writing—original draft preparation, F.S.A.-O.; writing—review and editing, F.S.A.-O., M.A.-Z.; visualization, F.S.A.-O.; supervision, M.A.M.R. and Y.A.A.-T.; project administration, M.A.M.R. and Y.A.A.-T.; funding acquisition, M.A.M.R. and Y.A.A.-T. All authors have read and agreed to the published version of the manuscript.

Funding: The project was funded by KAU Endowment (WAQF) at King Abdulaziz University, Jeddah, Saudi Arabia. The authors, therefore, acknowledge with thanks WAQF and the Deanship of Scientific Research (DSR) for technical and financial support.

Data Availability Statement: Data is contained within the article.

Conflicts of Interest: The authors declare no conflict of interest.

References

1. Wiser, R.; Rand, J.; Seel, J.; Beiter, P.; Baker, E.; Lantz, E.; Gilman, P. Expert elicitation survey predicts 37% to 49% declines in wind energy costs by 2050. *Nat. Energy* **2021**, *6*, 555–565. [CrossRef]
2. GWEC. GLOBAL WIND REPORT 2024. 2024. Available online: https://www.gwec.net/reports/globalwindreport/2024 (accessed on 11 April 2026).
3. McKenna, R.; Lilliestam, J.; Heinrichs, H.U.; Weinand, J.; Schmidt, J.; Staffell, I.; Hahmann, A.N.; Burgherr, P.; Burdack, A.; Bucha, M.; et al. System impacts of wind energy developments. *Joule* **2025**, *9*, 101799. [CrossRef]
4. Borissova, D.I.; Mustakerov, I.C. Designing of wind farm layout by using of multi-objective optimization. *Int. J. Math. Model. Methods Appl. Sci.* **2017**, *11*, 290–295.

5. Feng, J.; Shen, W.Z. Modelling Wind for Wind Farm Layout Optimization Using Joint Distribution of Wind Speed and Wind Direction. *Energies* **2015**, *8*, 3075–3092. [CrossRef]
6. Angelo, T.; Pierre-Elouan, R.; Gunner Chr, L. State of the Art of Wind Farm Optimization. In Proceedings of the EWEA 2012—European Wind Energy Conference & Exhibition, Copenhagen, Denmark, 16–19 April 2012.
7. Hidayat, T.; Ramli, M.A.M.; Alqahtani, M.M. Optimization of Non-Uniform Onshore Wind Farm Layout Using Modified Electric Charged Particles Optimization Algorithm Considering Different Terrain Characteristics. *Sustainability* **2024**, *16*, 2611. [CrossRef]
8. Long, H.; Zhang, Z.; Song, Z.; Kusiak, A. Formulation and Analysis of Grid and Coordinate Models for Planning Wind Farm Layouts. *IEEE Access* **2017**, *5*, 1810–1819. [CrossRef]
9. Wang, L.; Tan, A.C.; Gu, Y. Comparative study on optimizing the wind farm layout using different design methods and cost models. *J. Wind. Eng. Ind. Aerodyn.* **2015**, *146*, 1–10. [CrossRef]
10. Rodrigues, R.V.; Pedersen, M.M.; Schøler, J.P.; Quick, J.; Réthoré, P.-E. Speeding up large-wind-farm layout optimization using gradients, parallelization, and a heuristic algorithm for the initial layout. *Wind Energy Sci.* **2024**, *9*, 321–341. [CrossRef]
11. Mosetti, G.; Poloni, C.; Diviacco, B. Optimization of wind turbine positioning in large wind farms by means of a genetic algorithm. *J. Wind. Eng. Ind. Aerodyn.* **1994**, *51*, 105–116. [CrossRef]
12. Grady, S.A.; Hussaini, M.Y.; Abdullah, M.M. Placement of wind turbines using genetic algorithms. *Renew. Energy* **2005**, *30*, 259–270. [CrossRef]
13. Patel, J.; Savsani, V.; Patel, V.; Patel, R. Layout optimization of a wind farm using geometric pattern-based approach. *Energy Procedia* **2019**, *158*, 940–946. [CrossRef]
14. Wang, L. Comparative Study of Wind Turbine Placement Methods for Fla Wind Farm Layout Optimization with Irregular Boundary. *Appl. Sci.* **2019**, *9*, 639. [CrossRef]
15. Malisani, P.; Bartement, T.; Bozonnet, P. Offshore wind farm layout optimization with alignment constraints. *Wind Energy Sci.* **2025**, *10*, 1611–1623. [CrossRef]
16. Chowdhury, S.; Zhang, J.; Messac, A.; Castillo, L. Unrestricted wind farm layout optimization (UWFLO): Investigating key factors influencing the maximum power generation. *Renew. Energy* **2012**, *38*, 16–30. [CrossRef]
17. Feng, J.; Shen, W.Z. Solving the wind farm layout optimization problem using random search algorithm. *Renew. Energy* **2015**, *78*, 182–192. [CrossRef]
18. Kusiak, A.; Song, Z. Design of wind farm layout for maximum wind energy capture. *Renew. Energy* **2010**, *35*, 685–694. [CrossRef]
19. Yang, R.; Cui, T.; Chen, Z.; Ma, S.; Ping, H.; Wei, F.; Gao, Z.; Lu, G.; Liu, H.; Zhang, L. Review on Dynamic Inflow Sensing Layout Optimization for Large-Scale Wind Farms: Wake Modeling, Data-Driven Prediction, and Multi-Objective Uncertainty Optimization. *Energies* **2026**, *19*, 810. [CrossRef]
20. Huang, G.; Chen, Y.; Li, K.; Luo, J.; Zhang, S.; Lv, M. A Two-Step Grid–Coordinate Optimization Method for a Wind Farm with a Regular Layout Using a Genetic Algorithm. *Energies* **2024**, *17*, 3273. [CrossRef]
21. Spiru, P.; Paraschiv, L.S. Wind energy resource assessment and wind turbine selection analysis for sustainable energy production. *Sci. Rep.* **2024**, *10*, 10708. [CrossRef]
22. Barthelmie, R.J.; Jensen, L.E. Evaluation of wind farm efficiency and wind turbine wakes at the Nysted offshore wind farm. *Wind Energy* **2010**, *13*, 573–586. [CrossRef]
23. González-Longatt, F.; Wall, P.; Terzija, V. Wake effect in wind farm performance: Steady-state and dynamic behavior. *Renew. Energy* **2012**, *39*, 329–338. [CrossRef]
24. Jensen, N.O. *A Note on Wind Generator Interaction*; Risø National Laboratory: Roskilde, Denmark, 1983.
25. Circle-Circle Intersection. Available online: https://mathworld.wolfram.com/Circle-CircleIntersection.html (accessed on 11 April 2026).
26. Bouchekara, H. Electric Charged Particles Optimization and Its Application to the Optimal Design of a Circular Antenna Array. *Artif. Intell. Rev.* **2021**, *54*, 1767–1802. [CrossRef]
27. Hidayat, T.; Ramli, M.A.M.; Bouchekara, H.R.E.H.; Khalid, J.; Budiman, F.N. Design of 3D Wind Farm Layout Using an Improved Electric Charge Particles Optimization With Hub-Height Variety. *IEEE Access* **2022**, *10*, 31385–31396. [CrossRef]
28. Ramli, M.A.M.; Bouchekara, H.R.E.H.; Milyani, A.H. Wind farm layout optimization using a multi-objective electric charged particles optimization and a variable reduction approach. *Energy Strategy Rev.* **2023**, *45*, 101016. [CrossRef]
29. Choi, N.J.; Nam, S.H.; Jeong, J.H.; Kim, K.C. CFD study on aerodynamic power output changes with inter-turbine spacing variation for a 6 MW offshore wind farm. *Energies* **2014**, *7*, 7483–7498. [CrossRef]
30. Troen, I.; Lundtang Petersen, E. *European Wind Atlas*; Risø National Laboratory: Roskilde, Denmark, 1989; p. 656.

Disclaimer/Publisher's Note: The statements, opinions and data contained in all publications are solely those of the individual author(s) and contributor(s) and not of MDPI and/or the editor(s). MDPI and/or the editor(s) disclaim responsibility for any injury to people or property resulting from any ideas, methods, instructions or products referred to in the content.